Agricultural and Forest Meteorology 331 (2023) 109341

Contents lists available at ScienceDirect

Agricultural and Forest Meteorology

journal homepage: www.elsevier.com/locate/agrformet

Ecological restoration exacerbates the agriculture-induced water crisis in North China Region

Yan Zhou [a,b,c], Jinwei Dong [b,*], Yaoping Cui [a,c], Meng Zhao [d], Xinxin Wang [e], Qiuhong Tang [f], Yongqiang Zhang [f], Sha Zhou [g], Graciela Metternicht [h], Zhenhua Zou [i], Geli Zhang [j], Xiangming Xiao [k,*]

[a] Key Laboratory of Geospatial Technology for the Middle and Lower Yellow River Regions (Henan University), Ministry of Education, Kaifeng 475004, PR China
[b] Key Laboratory of Land Surface Pattern and Simulation, Institute of Geographic Sciences and Natural Resources Research, Chinese Academy of Sciences, Beijing 100101, PR China
[c] College of Geography and Environmental Science, Henan University, Kaifeng 475004, PR China
[d] Department of Earth and Spatial Sciences, University of Idaho, Moscow, ID 83844, USA
[e] Ministry of Education Key Laboratory of Biodiversity Science and Ecological Engineering, Institute of Biodiversity Science, Fudan University, Shanghai 200438, PR China
[f] Key Laboratory of Water Cycle and Related Land Surface Processes, Institute of Geographic Sciences and Natural Resources Research, Chinese Academy of Sciences, Beijing 100101, PR China
[g] Faculty of Geographical Sciences, Beijing Normal University, Beijing 100081, PR China
[h] School of Biological, Earth and Environmental Sciences, University of New South Wales, Sydney, NSW 2052, Australia
[i] Department of Geographical Sciences, University of Maryland, College Park, MD, 20742, USA
[j] College of Land Science and Technology, China Agricultural University, Beijing 100193, PR China
[k] Department of Microbiology and Plant Biology, and Center for Earth Observation and Modeling, University of Oklahoma, Norman, OK 73019, USA

ARTICLE INFO

Keywords:
North China Region
Sustainable development
Terrestrial water storage
Ecological restoration
Evapotranspiration

ABSTRACT

The North China Region (NCR), a typical grain base and highly populated area in China, is a well-recognized global groundwater funnel. Severe water shortage has been threatening and limiting sustainable development in the region over the past decades. Previous studies have reported the depleted water resources in the NCR and attributed the major driver to intensified agricultural water use, hardly considering the effects of the large-scale implementation of ecological restoration (ER) programs. As terrestrial water storage (TWS) is a critical indicator for measuring and evaluating regional water resources, understanding its spatial and temporal dynamics and responses to ER programs is significant for sustainable water management in the NCR. Here, we examine the interannual variations and trends of TWS in the NCR during 2002–2016 by using Gravity Recovery and Climate Experiment (GRACE) satellite data and the Google Earth Engine cloud computing platform. We find the significantly ($p < 0.01$) decreasing TWS (-8.9 mm/yr) and identify a hotspot with the most rapid depletion (-12.7±0.45 mm/yr) in the western NCR, where interannual variations and spatial patterns of TWS depletion are consistent with those of ER-induced greening. Attribution analyses of TWS depletion by considering precipitation, evapotranspiration, and runoff suggest increasing evapotranspiration induced by afforestation as the major driver for TWS depletion in the ER regions. Our study highlights ER is posing a new threat to water security in the NCR, and taking ecological water usage into account would be necessary for the synergy of food, water, and ecological securities and regional sustainable development.

1. Introduction

Water security is a global challenge (Aeschbach-Hertig and Gleeson 2012; He et al., 2021b; Rodell et al., 2018; Shen et al., 2022), particularly for China, a severe water-deficit country (7.7% of the global freshwater resources) with the largest population (18.5% of the world's population), fastest urbanization, growing economy, and water demand (He et al., 2021a; Ma et al., 2020; Tao et al., 2019). The uneven distribution of water resources further aggravates the water crisis in the country (Greve et al., 2018; Liu and Yang 2012; Wang et al., 2020). The

* Corresponding authors.
E-mail addresses: dongjw@igsnrr.ac.cn (J. Dong), xiangming.xiao@ou.edu (X. Xiao).

https://doi.org/10.1016/j.agrformet.2023.109341
Received 11 August 2022; Received in revised form 4 December 2022; Accepted 20 January 2023

North China Region (NCR) is home to 26% of the human population in China and provides 25% of the national food production and gross domestic product (GDP), but has only 3% of the national freshwater resources (Zhou et al., 2022). Thus, detailed information about the spatial-temporal dynamics of water storage over the past decades is critical to accurately predicting water resource changes and taking adaptive water management measures to sustainably utilize water resources in the NCR (Liu and Yang 2012; Wang et al., 2020; Zhou et al., 2022).

Previous studies have identified the most serious depletion hotspots of water storage in the world, including the NCR, Northwest India Plain, and U.S. High Plain (Aeschbach-Hertig and Gleeson 2012; Asoka et al., 2017; Huang et al., 2015; Rodell et al., 2018), using the gravity recovery and climate experiment (GRACE) satellite data which record the monthly changes in terrestrial water storage (TWS) which represents the sum of surface water, soil water, groundwater, ice, snow, and vegetation water (Meng et al., 2019; Rodell et al., 2009). Although the variations of groundwater levels can be locally and accurately measured by wells (Aeschbach-Hertig and Gleeson 2012), monitoring the large-scale changes in groundwater storage and TWS is mostly realized based on the direct observations from GRACE satellite (Döll et al., 2014; Dong et al., 2022). The depletion of TWS in the NCR has been attributed to intense agricultural irrigation from groundwater pumping in the past decades (Aeschbach-Hertig and Gleeson 2012; Pan et al., 2017; Qin et al., 2013). For example, Huang et al. (2015) revealed that excessive pumping for irrigation caused severe groundwater storage decline (~ 16 mm/yr in 2003–2013) in the central and eastern parts of the NCR by isolating groundwater storage from TWS using land surface models (Noah, Mosaic, Community Land Model, and Variable Infiltration Capacity) driven by global land data assimilation system (GLDAS) version 1. Koch et al. (2020) estimated an average annual net irrigation of 126 mm/yr (15.2 km^3/yr) for the NCR using a remote sensing-based model (i.e., Priestly-Taylor Jet Propulsion Laboratory) and a hydrologic model (multiscale Hydrologic Model). However, agricultural water use may decrease with the implementation of water-saving irrigation technology and cropland loss due to the launch of ecological restoration (ER) programs (Bryan et al., 2018; Li et al., 2020a; Liu et al., 2008; Lu et al., 2018; Wei et al., 2019; Zuo et al., 2018). In contrast, the amount of water used by other sectors (e.g., ecological water consumption as reforestation) could increase and cause significant effects on TWS (Feng et al., 2016; Zhao et al., 2021). Therefore, the changes in the water use structure might have led to the changes in driving factors of regional TWS dynamics in the NCR.

Water consumption from large-scale ER programs has been considered a significant anthropogenic contributor to TWS changes in some typical regions in the world, especially in Northern China (Bai et al., 2020; Feng et al., 2016; Li et al., 2020a; Shao et al., 2019; Zhao et al., 2021). While previous studies have reported that China led in the greening of the world due to ecological conservation and land management in the past two decades (Chen et al., 2019a; Li et al., 2018; Zhu et al., 2016), several recent studies (Bai et al., 2020; Feng et al., 2016; Li et al., 2020a; Shao et al., 2019; Zhao et al., 2021) have proved that the continuous increase of evapotranspiration (ET) induced by the implementation of ER programs has exerted excessive pressure on regional water resources, such as the Loess Plateau (Feng et al., 2016; Shao et al., 2019) and Mu Us Sandyland (TWS depletion rate: 16.6 ± 5.0 mm/yr) (Zhao et al., 2021) of China. The western part of NCR is one of the core regions of ER that has been implementing the Grain to Green Program and Natural Forest Conservation Program on a large scale since 1999 (Bryan et al., 2018; Li et al., 2020a; Liu et al., 2008; Lu et al., 2018; Ouyang et al., 2016; Zuo et al., 2018). However, it is still unclear how these afforestation processes would affect the extremely limited water resources in the region. Therefore, it will be of great significance to quantitatively analyze the effects of large-scale ER programs on TWS changes in the NCR by fully considering and using the indicators related to land use changes, human activities, and climate change.

This study aimed to detect the hotspots that experienced the most drastic TWS changes and ER in the NCR and examine to which extent the pending ER programs would affect regional water storage. To achieve this objective, we firstly investigated the spatial-temporal patterns of TWS changes in the NCR during 2002–2016 by using GRACE mascon data, and identified the hotspot of water storage depletion; secondly, we explored the spatial and temporal consistency between TWS depletion and ER programs by integrating the changes of land use, human activities, and climate factors; finally, we clarified the effects of ER programs on TWS loss in the hotspot from the perspective of water balance, by considering the changes in annual precipitation, ET, runoffs, and agricultural water use before (1980–1999) and during ER programs (1999–2018). This study is expected to provide an updated understanding of water storage changes and their driving mechanisms in the NCR, and warn the possible water risks of ER programs in other similar regions worldwide. It would shed light on the synergies of food, water, and ecological securities, and guide decision-making for sustainable management of extremely limited water resources.

2. Materials and methods

2.1. Study area

The NCR is one of the major populous, economic, industrial, and agricultural centers in China. It geographically includes the municipalities of Beijing and Tianjin and the provinces of Hebei, Henan, Shandong, and Shanxi. Considering the smaller areas of Beijing and Tianjin Municipality compared to other provinces, they were merged as one region (Beijing-Tianjin, B&T) in this study. The NCR covers an area of about 700,000 km^2 (7% of China's land area) and is one typical region with a dense population (26% of China's population) and intensive agriculture and strong industry (25% of national grain production and GDP) in China (Fig. 1a). However, it contains only 3% of the total national water resources. Groundwater accounts for 60% of the freshwater resources and has become an indispensable factor to support the socioeconomic development of the NCR (Qin et al., 2013). Since the mid-1960s, extensive pumping for agricultural irrigation has caused severe groundwater depletion in the NCR (Han et al., 2017). However, rapid population growth and urbanization will consume more freshwater resources, and the socioeconomic development in the region is likely to be limited by water scarcity (Qin et al., 2013).

2.2. Data

2.2.1. GRACE TWS data

We used three GRACE Release-06 mascon products provided by the University of Texas center for space research (CSR), national aeronautics and space administration (NASA) Jet Propulsion Laboratory (JPL), and Deutsches geoforschungszentrum (GFZ) to detect the changes in TWS during 2002–2016 (Table 1). The previous study suggested that an arithmetic mean of these data products could effectively reduce the noise in the gravity field solutions (Sakumura et al., 2014). The grid size and temporal resolution of the three data sets are 1° and one month, respectively. All these three GRACE datasets have been released and stored in the Google Earth Engine (GEE) cloud data archive (GEE asset address: NASA/GRACE/MASS_GRIDS/LAND). For each GRACE mascon solution, the monthly estimates are anomalies of the total terrestrial water mass relative to mean values from 2004 to 2010 (refers to GRACE data description in https://developers.google.com/earth-engine/datasets/catalog/NASA_GRACE_MASS_GRIDS_MASCON). In this study, the trends in annual TWS were derived using the following steps based on the GEE platform. For each GRACE mascon solution, the months with missing values were filled by linear interpolation based on the data corresponding to the previous and following months (Ramillien et al., 2006). The monthly GRACE estimates used in this study were derived by averaging the three GRACE products. For each pixel, the TWS in a year

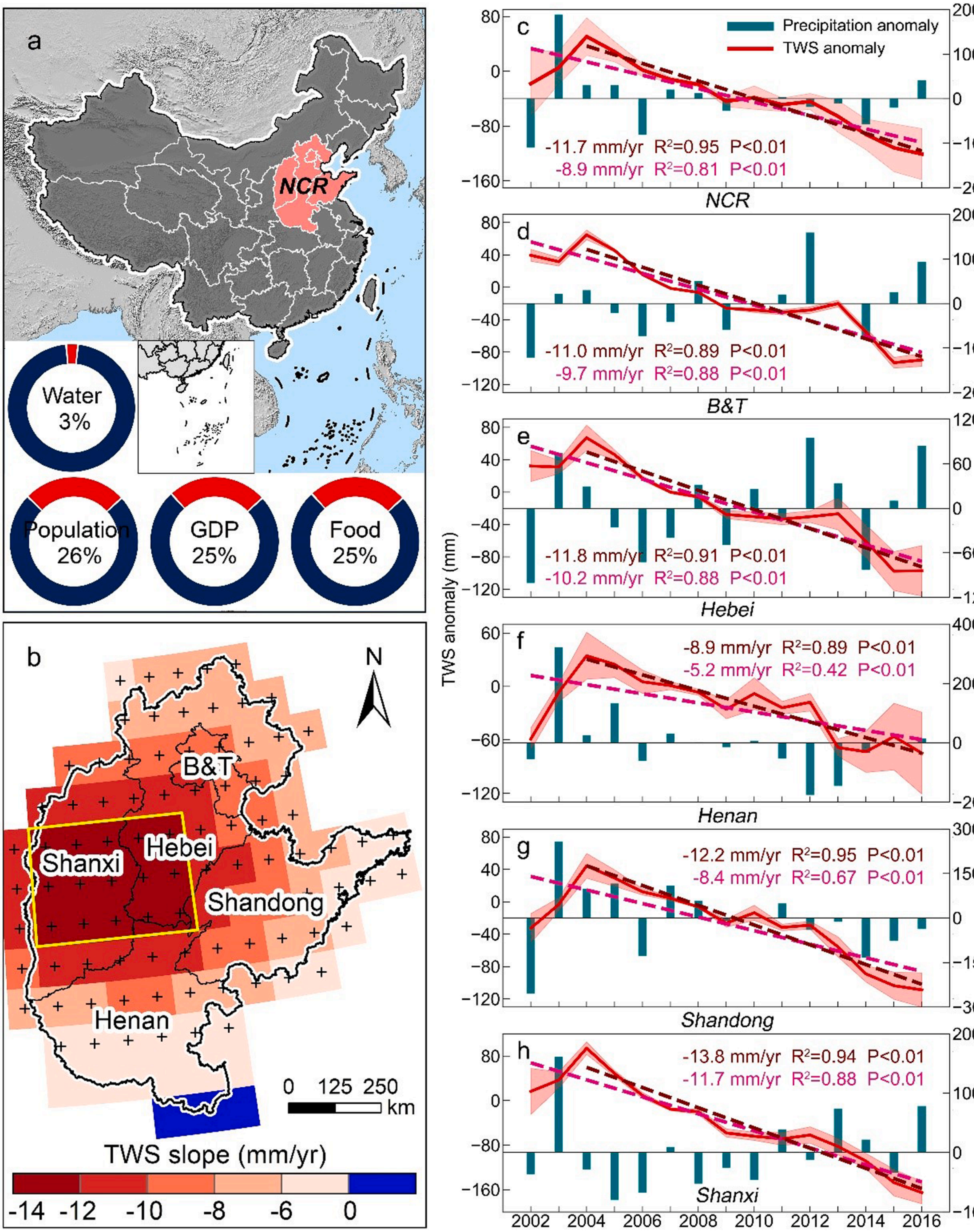

Fig. 1. Variations and trends of terrestrial water storage (TWS) in the North China Region (NCR). (a) Spatial patterns of freshwater resources per capita in China and the percentages of the total human population, gross domestic product (GDP), and food production in the NCR relative to the entire country in 2019; (b) Spatial patterns of linear trends of TWS in the NCR during 2002–2016; (c–h) Interannual variations and linear trends of TWS in the entire NCR (c) and different municipalities and provinces (d: B&T; e: Hebei; f: Henan; g: Shandong; h: Shanxi) during 2002–2016. The symbol "+" in each grid cell indicates a statistically significant trend with a p-value < 0.05. The purple and dark red dotted lines represent the linear regressions of inter-annual variations of TWS during 2002–2016 and 2004–2016, respectively.

Table 1
A detailed summary of the raster data related to TWS, land use and land cover, human activities, ecological indicators, and climate factors used in this study.

Data	Pixel size	Temporal resolution	Temporal span	Source
TWS				
CSR GRACE	1o	Monthly	2002–2017	https://grace.jpl.nasa.gov/data/get-data/monthly-mass-grids-land/
JPL GRACE	1o	Monthly	2002–2017	
GFZ GRACE	1o	Monthly	2002–2017	
Land use and land cover				
NLCD-China	100 m	Five years	1980–2020	(Liu et al., 2003; Liu et al., 2018)
GAIA	30 m	Yearly	1985–2018	(Gong et al., 2020)
Water map	30 m	Yearly	1987–2020	(Zhou et al., 2022)
Human activity				
DMAP NTL	30″	Yearly	1992–2018	(Li et al., 2020b)
WorldPop	100 m	Yearly	2020–2021	https://hub.worldpop.org/project/categories?id==3
Ecological indicators				
MOD13A1	500 m	16 days	2000–	https://lpdaac.usgs.gov/products/mod13a1v006/
GIMMS-3 g	0.083o	15 days	1981–2015	https://data.tpdc.ac.cn/en/data/9775f2b4-7370-4e5e-a537-3482c9a83d88/
GLASS	0.05o	8 days	1981–2018	(Liang et al., 2013)
GLOBMAP-V3	0.073o	16 days (1981–2000)8 days (2001–2019)	1981–2019	(Chen et al., 2019b; Liu et al., 2012)
LAI3g	0.083o	15 days	1981–2016	(Zhu et al., 2013)
MOD16	1000 m	8 days	2000–	https://modis.gsfc.nasa.gov/data/dataprod/mod16.php
PML_V2	500 m	8 days	2000–2020	(Zhang et al., 2019)
GLEAM	0.25o	Daily	1980–2018	(Martens et al., 2017)
Climate factors				
CMA	0.25o	Monthly	1981–2020	http://data.cma.cn/
CRU TS	0.5o	Monthly	1981–2020	https://crudata.uea.ac.uk/cru/data/hrg/
TRMM	0.25o	Monthly	1998–2019	https://gpm.nasa.gov/data/directory
ERA5	0.25o	Monthly	1979–2021	https://www.ecmwf.int/en/forecasts/datasets/reanalysis-datasets/era5
CMIP5	0.25o	Daily	2020–2099	https://developers.google.com/earth-engine/datasets/catalog/NASA_NEX-GDDP

was calculated by averaging the GRACE estimates of the 12 months in that year.

2.2.2. Land use and land cover data

The land use and land cover data sets used in this study were the NLCD-China (Table 1), collected from the Institute of Geographic Sciences and Natural Resources Research, Chinese Academy of Sciences (Liu et al., 2003; Liu et al., 2018). The data sets were generated at a five-year interval with satisfactory overall accuracies higher than 92.0% (Liu et al., 2003; Liu et al., 2018), by interpreting the information on land use changes based on the images from Landsat and other satellites (CBERS-2 and Gaofen-1/2). Two-period land cover data from 2000 to 2015 was used to investigate the spatial patterns of the intensity of ER and changes in cropland areas in the NCR. Global artificial impervious area (GAIA) data for 1985–2018 generated by Tsinghua University with a spatial resolution of 30 m were employed to depict the spatial patterns of changes in impervious surfaces (Gong et al., 2020). The data were produced with a mean overall accuracy higher than 90.0%, by using time-series Landsat, Sentinel-1, and nighttime light (NTL) data and the GEE cloud computing platform. Surface water area (SWA) was obtained from the annual 30-m water body maps with overall accuracies higher than 96.0% in the NCR from 1987 to 2020 in our previous study (Zhou et al., 2022). The data were generated using all the available Landsat imagery, water indices- and threshold-based water mapping algorithm, and the GEE.

2.2.3. Human activity and water use data

The intensities of human activities were reflected by the NTL index and human population (Table 1). NTL data used in the current study were collected from global DMSP NTL time-series data, which was generated by harmonizing the inter-calibrated NTL observations from the DMSP data and the simulated DMSP-like NTL observations from the VIIRS data (Li et al., 2020b). The generated global DMSP NTL time-series data can provide valuable support for studies related to human activities, including urban extent dynamics (Bennett and Smith 2017; Zhao et al., 2020; Zhou et al., 2018). Although there are inevitable uncertainties in NTL pixels with digital number values lower than 10, the impact on the applications of DMSP NTL data is limited because zones with high luminance are always paid more attention (Li et al., 2020b). Annual global human population maps for 2000–2021 produced by the WorldPop project (https://www.worldpop.org) with a spatial resolution of 100 m were employed to study the spatial and temporal changes in the human population in the NCR.

Annual human water use data including the sectors of agricultural, industrial, and residential water use in different provinces in the NCR during 2002–2016 were collected from the Water Resources Bulletin of each region, namely: Beijing Water Resources Bulletin (http://swj.beijing.gov.cn/zwgk/szygb/), Tianjin Water Resources Bulletin (http://swj.tj.gov.cn/gztb_17212/index.html), Hebei Water Resources Bulletin (http://slt.hebei.gov.cn/dynamic/search.js), Henan Water Resources Bulletin (http://slt.henan.gov.cn/bmzl/szygl/szygb/), Shandong Water Resources Bulletin (http://wr.shandong.gov.cn/zwgk_319/szygb/), and Shanxi Water Resources Bulletin (http://slt.shanxi.gov.cn/zncs/szyc/szygb/). In addition, we obtained data on annual irrigation water use in the Fenhe River Basin in Shanxi Province during 1980–2013 from Zhou et al. (2020).

2.2.4. Data of ecological indicators

Normalized Difference Vegetation Index (NDVI) data used in the study were from the two data sets of MOD13A1 (2000–, 500 m, and 16 days) and GIMMS-3 g (1981–2015, 0.0833°, and 15 days) (Table 1). Three kinds of Leaf Area Index (LAI) data sets were used, namely: GLASS, GLOBMAP-V3, and LAI3g. These three LAI data sets were generated using the processed Advanced Very High Resolution Radiometer (AVHRR) data, in which the possible errors have been fully considered and rectified, such as the degradation and inter-calibration of the AVHRR sensors and changes in sun-target-view geometry caused by orbital drift (Chen et al., 2019b; Tucker et al., 2005). For GLOBMAP-V3 datasets, the temporal coverage is from 1981 to 2019 (http://globalmapping.org/globalLAI/), the spatial resolution is 0.072727°, and the temporal resolutions vary from 16 days during 1981–2000 to 8 days during 2001–2019 (Chen et al., 2019b; Liu et al., 2012). For GLASS products, the temporal coverage is from 1981 to 2018 (http://www.glass.umd.edu/Download.html), and the spatial and temporal resolutions are 0.05° and 8 days, respectively (Liang et al., 2013). For LAI3g data sets, the temporal coverage is from 1981 to 2016, (https://drive.google.com/open?id=0BwL88nwumpqYaFJmR2poS0d1ZDQ), and the spatial and temporal resolutions are 0.0833° and 15 days, respectively (Zhu et al., 2013). Three kinds of time-series ET data sets were used, namely: MOD16, Penman-Monteith-Leuning (PML_V2), and the Global

Land Evaporation Amsterdam Model (GLEAM) V3.3a. For MOD16, the temporal coverage is from 2000 to the present, and the spatial and temporal resolution are 1000 m and 8 days, respectively. For PML_V2 data sets, the temporal coverage is from 2000 to 2020, and the spatial and temporal resolution are 500 m and 8 days (Zhang et al., 2019), respectively. For GLEAM V3.3a data sets, the temporal coverage is from 1980 to 2018, and the spatial and temporal resolution are 0.25° and daily (https://www.gleam.eu/) (Martens et al., 2017), respectively. Previous studies (Jia et al., 2022; Zhang et al., 2019) have demonstrated the applicability of GLEAM and PML_V2 ET data sets in water balance analyses because they are closest to the observations from the eddy covariance flux tower. In addition, we also used the different layers in PML_V2 data sets to investigate the interannual variations and spatial patterns of linear trends of surface water evaporation, plant transpiration, soil evaporation, and interception loss in the NCR during 2002–2016.

2.2.5. Climatic and hydrological data

In this study, four kinds of long-term climate data sets were used to examine the trends of annual precipitation in the study area (Table 1), namely: the monthly 0.25° gridded precipitation data from the China Meteorological Administration (CMA), the monthly 0.5° precipitation data from the Climatic Research Unit Timeseries (CRU TS) version 4.01, the monthly 0.25° precipitation data from the Tropical Rainfall Measuring Mission (TRMM), and the monthly 0.25° precipitation data from ERA5. Especially, Zhao et al. (2021) has confirmed the feasibility of using CRU TS precipitation data set to conduct water balance analyses in Northern China. The data sets of CMA, CRU TS, and ERA5 were applied to analyze the trends of annual mean temperature. Future climate trends were investigated by using the projected climate change data set in the 21st century with the spatial and temporal resolutions of 0.25° and daily, which were derived from Coupled Model Intercomparison Project Phase 5 (CMIP5) climate model under two Representative Concentration Pathway (RCP) scenarios: the medium greenhouse gas emission scenario RCP 4.5 and high emission scenario RCP 8.5 (https://esgf-node.llnl.gov/search/cmip5/). Based on the CMIP5 data set, annual precipitation and annual mean temperature in the study area from 2020 to 2099 were calculated. We obtained annual runoff data for the Fenhe River Basin for 1980–2018 from the Hejin Hydrological Station.

2.3. Methods

2.3.1. Trend analyses of TWS and other indicators

Based on annual maps of TWS anomalies with a grid size of 1°, we firstly applied the Theil-Sen slope estimator and the Mann-Kendall test method to annual TWS anomaly maps to calculate the slope of TWS and its statistical significance level in each pixel from 2002 to 2016. The median-based non-parametric slope estimation model of Theil-Sen has no strict requirement for specific data distribution (Yang et al., 2019). The Mann-Kendall trend test method is also non-parametric and has been widely used to analyze the trends of indicators in the field of geoscience (Forkel et al., 2015; Wang et al., 2018; Yang et al., 2019). Then, we investigated the interannual variations and trends of TWS in the NCR during 2002–2016 at both the provincial and prefectural scales using the Python 3.9 programming language and ArcGIS 10.5 software platform. Similarly, we investigated the interannual variations and linear trends of other factors related to land use (e.g., surface water areas), climate change (e.g., annual precipitation), and human activity (e.g., total population) at both the pixel and regional scales.

2.3.2. Attribution analyses of TWS depletion based on turning point matching

Based on the spatial patterns of linear trends of TWS in the NCR from 2002 to 2016, we found the hotspot with the most rapid decreases in TWS in the central part of Shanxi Province, which has been experiencing large-scale ER since 1999. To reveal the effects of ER on TWS, firstly, we compared the spatial patterns of linear trends of TWS and ecological indicators (i.e., NDVI, LAI, and ET), and found the significant and most rapid increases of NDVI, LAI, and ET in the hotspot. Secondly, we investigated and compared the interannual variations of NDVI, LAI, and ET in both the regions of ER and croplands, and found that NDVI, LAI, and ET in the ER regions showed decreasing trends before 1999 while continuously increasing trends during 1999–2018. The same trends and time turning points for NDVI, LAI, and ET suggested that improving vegetation conditions significantly contributed to the increase of ET in the ER regions since 1999. Similarly, we carried out the same analyses of NDVI, LAI, and ET in the hotspot like that in all the regions of ER, and also found the decreases of NDVI, LAI, and ET before 1999 while continuous increases in these three indicators after 1999.

2.3.3. Attribution analyses of TWS depletion based on water balance analyses

The change analyses of TWS from the perspective of water balance are generally conducted at the watershed scale. In this study, we took the Fenhe River Basin, which is located in the central part of the hotspot of TWS decline, as an example, to quantitatively explored the effects of ET, precipitation, and runoff on TWS changes. Firstly, we investigated the interannual variations of annual precipitation, ET, and runoff from 1980 to 2018. Then, we compared the average annual values of precipitation, ET, and runoff in the basin before and after ER programs to determine the possible factors leading to the continuous decline of TWS from 2002 to 2016. Finally, we applied partial correlations to quantitatively explore the effects of the three factors on TWS dynamics.

2.3.4. Delineation of regions of ER and permanent agriculture

According to the characteristics of land use in China, we separated the regions of ER and permanent agriculture at the spatial resolution of 1 km to ensure the spatial continuity of the same type of land and avoid fragmentation of land use classification (Liu et al., 2014; Liu et al., 2010) (Fig. S1). Firstly, we investigated the spatial distributions of forests and croplands in 2000 and 2015 based on the land cover maps (NLCD-China) with a grid size of 100 m. Secondly, we aggregated the maps of forests and croplands into area percentage maps of forests and croplands at 1 km resolution. In terms of the definition of ER regions, the pixels that meet the criterion $Ratio_{(F,2015)}$ - $Ratio_{(F,2000)} \geq 1\%$ were identified as ER regions (see Text S1 for details), in which $Ratio_{(F,2000)}$ *and* $Ratio_{(F,2015)}$ represent the ratio of forest area in each grid cell in 2000 and 2015, respectively. In terms of the definition of permanent agricultural regions, a criterion $Ratio_{(C,2000)} \geq 50\%$ & $Ratio_{(C,2015)} \geq 50\%$ was used to identify the pixels of permanent agriculture (see Text S2 for details), in which $Ratio_{(C,2000)}$ *and* $Ratio_{(C,2015)}$ represent the ratio of cropland area in each grid cell in 2000 and 2015, respectively.

3. Results

3.1. Depleted water storage in the NCR from 2002 to 2016

Generally, TWS showed continuously decreasing trends in the NCR from 2002 to 2016. Specifically, among the 101 grid cells of annual TWS anomaly maps with a spatial resolution of 1°, 92 (91%) of them experienced significant ($p < 0.05$) decreases in TWS during 2002–2016 (Fig. 1b). The most severe decline of TWS (−12.7±0.45 mm/yr) was found in the western part of NCR (especially in the central part of Shanxi Province), which included 15 GRACE pixels (14.9% or 18.5 million ha) and was the hotspot of depleted TWS (hereafter called hotspot) identified in this study. The TWS depletion outside the hotspot was milder, and the southern part of Henan Province and the eastern part of Shandong Province showed the lowest decline rates. In terms of the interannual variations and trends of TWS, the regional average TWS significantly decreased at a rate of 8.9 mm/yr in the NCR during the period (Fig. 1c). At the provincial scale, we found that Shanxi Province experienced the most rapid loss of TWS, with the rates of 11.7 mm/yr during 2002–2016 and 13.8 mm/yr during 2004–2016, respectively (Fig. 1h).

It was worth noting that there was a sharp increase in TWS (62.8 mm) in the NCR from 2002 (−3.9 mm) to 2004 (58.9 mm), and then it substantially decreased at a rate of 11.7 mm/yr during 2004–2016 (Fig. 1c). Therefore, the declined rate (11.7 mm/yr) of TWS in the NCR during 2004–2016 was higher than that (8.9 mm/yr) during 2002–2016. Interannual variations and trends of TWS in each province were similar to those in the whole NCR (Fig. 1d–h). The large-scale implementation of water projects could contribute to the sharp increase in TWS during some periods. For example, the Ecological Urgent Water Replenishing project, which diverted water from the Yangtze River to sustain Lake Nansihu (Huang 2003; Wang et al., 2020), was implemented in Shandong Province in 2002 to alleviate severe drought (Fig. S2). Other water projects could also lead to the periodic elevation of TWS, such as the Yellow River Diversion project in Shanxi Province since 2002 (Zhou et al., 2022) and the South-to-North Water Diversion project in the provinces of Henan, Hebei, and Shandong since 2014 (Long et al., 2020).

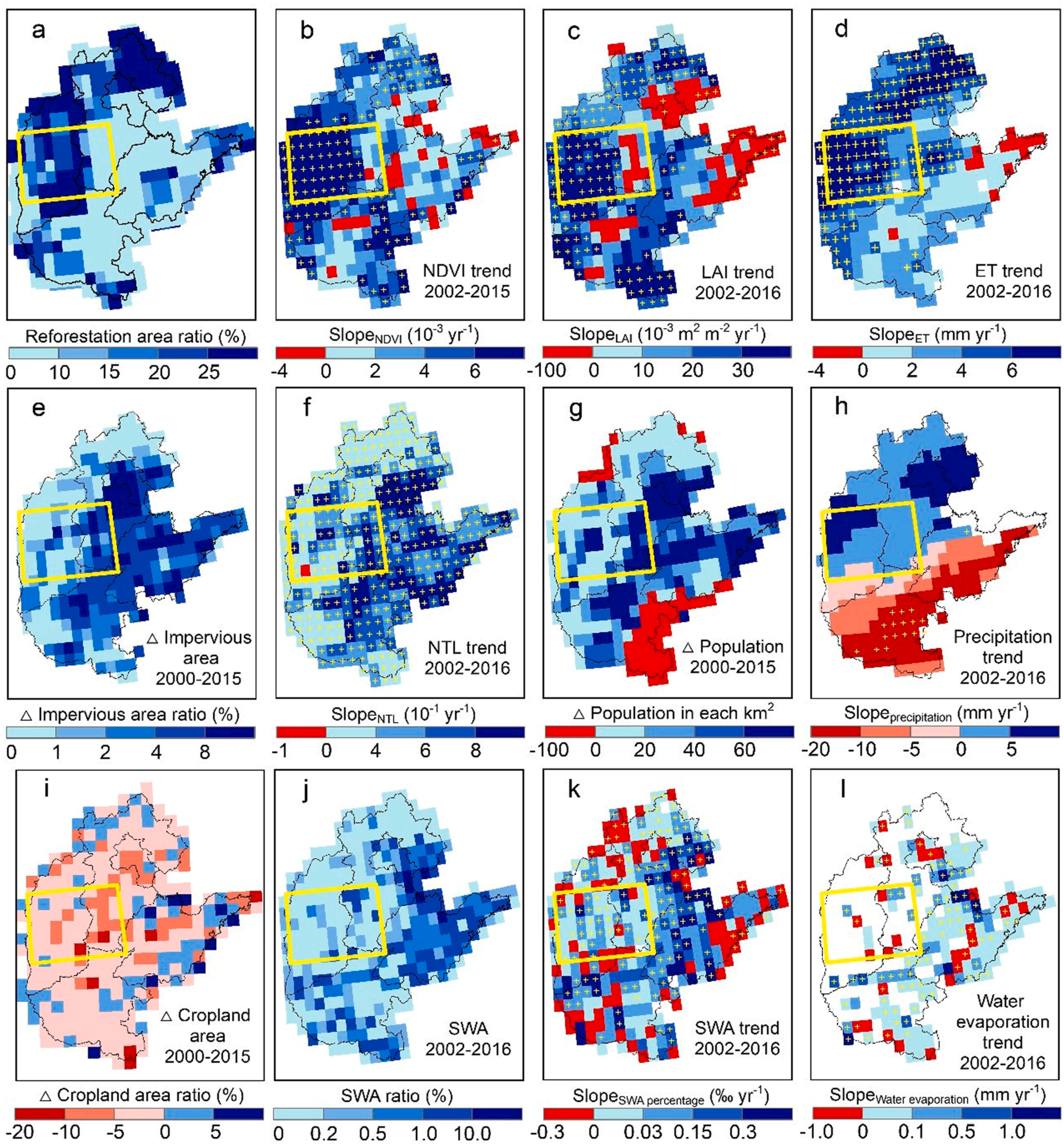

Fig. 2. Spatial patterns of changes in land use, human activities, and climate in the NCR. (a) Reforestation intensity; (b–d) Linear trends of Normalized Difference Vegetation Index (NDVI), Leaf Area Index (LAI), and evapotranspiration (ET); (e) Impervious area change; (f) Linear trends of nighttime light (NTL) index; (g) Population change; (h) Linear trends of annual precipitation; (i) Cropland area change; (j) Average annual surface water area (SWA); (k–l) Linear trends of annual SWA and water evaporation. The symbol "+" in each grid cell indicates a statistically significant trend with a p-value < 0.05.

3.2. Attribution analyses of water storage depletion to ER

We examined the spatial patterns of changes in the factors related to land use, human activities, and climate with a spatial resolution of 0.5° × 0.5° We found substantial reforestation in the western (i.e., Shanxi Province) and northern parts of NCR (Fig. 2a) due to the large-scale implementation of ER programs (i.e., Grain to Green Program and Natural Forest Conservation Program). By investigating the spatial patterns of linear trends of NDVI (mean of GIMMS-3 g and MOD13A1), LAI (mean of GLASS, GLOBMAP, and LAI3g), and ET (mean of GLEAM, PML-V2, and MOD16), we found the most rapid increases of the three indicators in the hotspot (Fig. 2b–d). Each dataset also showed the most rapid increases in NDVI, LAI, and ET in the hotspot (Figs. S3–S5). On the contrary, the increases in artificial impervious surface areas, NTL, and human population (Fig. 2e–g) in the western NCR were much lower than those in the central and eastern parts, suggesting weaker human activities in the western NCR. Most grid cells experienced significant decreases in cropland areas (Fig. 2i), which was consistent with the decreases in agricultural water use in the NCR (Fig. 3). Although agricultural water use in Shanxi Province showed a slightly increasing trend (0.6 mm/yr), its average annual value (23.3 mm) was much less than that in other provinces (Beijing-Tianjin: 68.4 mm; Hebei Province: 78.7 mm; Henan Province: 76.1 mm; Shandong Province: 100.6 mm). To further demonstrate better vegetation growth while weaker human activities in the western NCR, we investigated and compared the areas of croplands and forests, ET, and human population in each prefecture. Taking 2015 as an example, the results showed that compared with other regions, the forest densities and ET in the prefectures in Shanxi Province were higher, while the cropland areas and human population were relatively smaller (Fig. S6). In addition, the prefectures in Shanxi experienced a more severe TWS decline. Generally, rapid reforestation dominated the patterns of land use changes in the western NCR, while urbanization happened in the whole plain, especially in the eastern NCR.

Annual precipitation showed increasing trends in the hotspot and even the whole northern NCR (Fig. 2h), which suggested that the precipitation change is not the major driver for rapid TWS decline in the hotspot. Human water use data showed that agricultural water use was the largest sector of water consumption in the NCR except for beijing & tianjin (B&T), especially in the provinces of Hebei, Henan, and Shandong, which are typical agricultural production bases (Fig. 3), agreeing

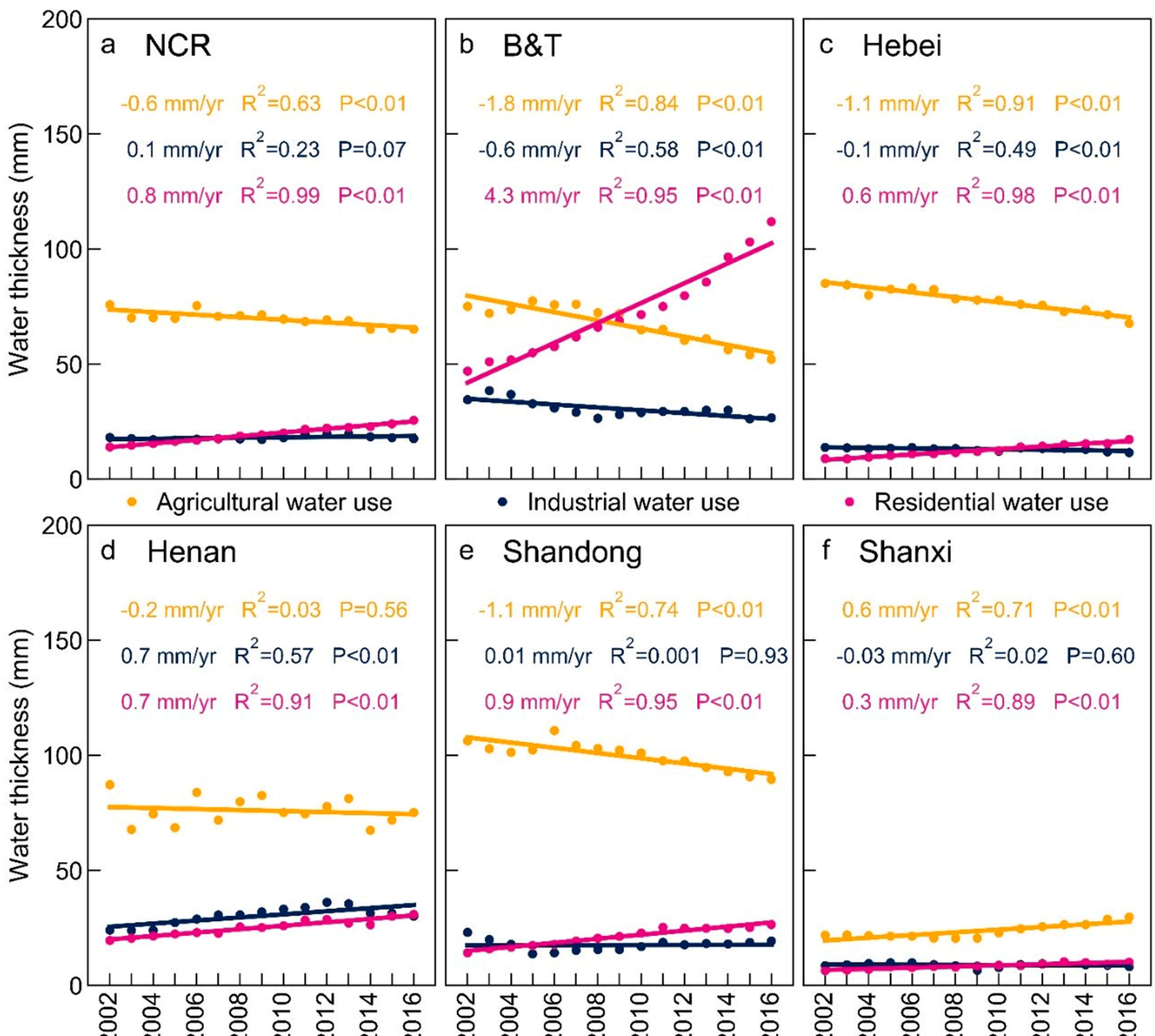

Fig. 3. Trends and linear regression of annual agricultural water use, industrial water use, and residential water use in the whole NCR (a) and different provinces (b–f).

well with the findings in previous studies that evaporation from agricultural irrigation greatly contributed to TWS decline in these regions (Aeschbach-Hertig and Gleeson 2012; Huang et al., 2015; Pan et al., 2017; Qin et al., 2013; Xu et al., 2019). Though Shanxi Province experienced the most rapid decline of TWS among all the provinces, its agricultural water use was much lower than that in other provinces, which suggested that evaporation from agricultural irrigation could not be the largest contributor to ET increases in Shanxi. While the hotspot had the most rapid increase in ET, its surface water area (SWA) was much lower than other regions (Fig. 2j). In addition, the increasing rates of SWA and water evaporation in the hotspot were also much lower than those in the eastern NCR (Fig. 2j-l), which indicated that the changes of water evaporation were also not the major driver of ET increases in the hotspot. An interesting phenomenon was that the most rapid increase of SWA occurred in Shandong Province where annual precipitation showed decreasing trends. Our previous study (Zhou et al., 2022) has reported that the rapid expansion of SWA in Shandong Province in the past decades was mainly caused by anthropogenic factors (i.e., constructing artificial lakes and coastal aquaculture ponds), rather than climate change.

To further confirm the hypothesis that reforestation led to the rapid increases of ET in ER regions, we analyzed the changes of NDVI (GIMMS-3 g), LAI (the mean of GLASS, GLOBMAP, and LAI3g), and ET (GLEAM) in the regions of ER and agriculture (see *Methods* and Fig. S1 for detailed definition). The results showed that NDVI, LAI, and ET in the reforestation region showed decreasing trends (NDVI: −0.001/yr; LAI: −0.01 m^2/m^2/yr; ET: −6.34 mm/yr) before ~1999 and followed by significantly increasing trends (NDVI: 0.007/yr; LAI: 0.03 m^2/m^2/yr; ET: 6.57 mm/yr) (Fig. 4a–c). The same turning point for the three indicators around 1999 (start time of the ER programs) suggested that ER has significantly improved vegetation growth and consequently led to increases in ET. However, the increases in NDVI (0.001/yr), LAI (0.019 m^2/m^2/yr), and ET (1.68 mm/yr) in the croplands (1990–2018) were much lower than those in the ER regions (Fig. 4g–i). As ET is the result of soil evaporation, vegetation transpiration, and canopy interception loss, here we also investigated their trends in the ER regions during 2000–2018 by using different data layers in PML-V2 datasets. We found that vegetation transpiration continuously and rapidly increased (5.94 mm/yr) during the period (Fig. 4d). The magnitude of canopy interception loss (0.61 mm/yr) was minor compared to vegetation transpiration (Fig. 4e). The decline in soil evaporation (2.27 mm/yr) was consistent with the decrease in croplands (Fig. 4f). Therefore, the increased reforestation-induced vegetation transpiration was the largest contributor to ET increases in the ER regions.

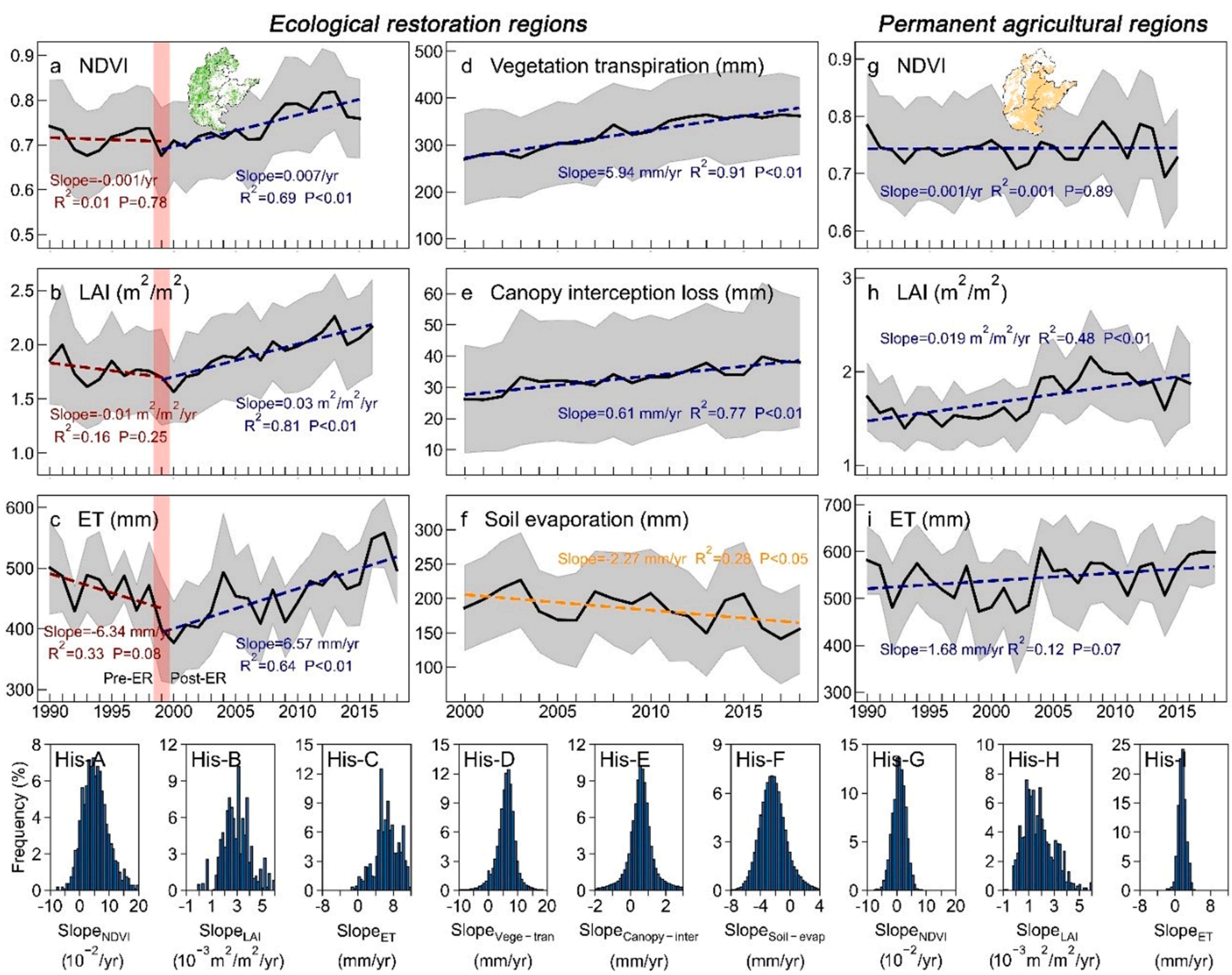

Fig. 4. Variations and trends of NDVI, LAI, and ET in the regions of ER and agriculture. (a–c) Interannual variations and trends of NDVI (GIMMS-3 g), LAI (mean of GLASS, GLOBMAP, and LAI3g), and ET (GLEAM) in the ER regions during 1990–2018; (d–f) Interannual variations and trends of vegetation transpiration, canopy interception loss, and soil evaporation derived from PML-V2 datasets in the ER regions during 2000–2018; (g–i) Interannual variations of NDVI, LAI, and ET in the croplands during 1990–2018. The below shows the histograms (a–i) of the slopes in the linear trends (a–c: 1999–2018; d–f: 2000–2018; g–i: 1990–2018) of these indicators.

3.3. Impacts of ER on TWS from a perspective of water balance

To attribute the decreasing TWS in the hotspot, here we took the Fenhe River Basin, which is in the center of the hotspot and accounts for 25% of the area of Shanxi Province (Fig. 5a), to analyze the effects of ET increases on TWS decline, from a perspective of water balance. The variations and trends of annual precipitation, runoff, and ET in the region from 1980 to 2018 were shown in Fig. 5b–d. The average annual precipitation during ER programs (510.3 mm/yr) was higher than that before ER (476.1 mm/yr), while the average annual runoff during ER (12.9 mm/yr) was lower than that before ER (16.6 mm/yr), which were favorable to the recovery of TWS. Though runoff showed a slightly increasing trend (0.8 mm/yr) from 2002 to 2016, the average annual value of runoff (12.9 mm) was much lower than that of precipitation (510.3 mm). Therefore, the effects of changes in the runoff on TWS variations could be almost neglected. However, the average annual ET during ER (GLEAM: 457.8 mm/yr) was higher than that before ER (GLEAM: 428.2 mm/yr), and annual ET showed continuously increasing trends (GLEAM: 5.4 mm/yr; PML_V2: 5.4 mm/yr) during the ER period, which suggested that TWS decline could be caused by ET increase. To further confirm our inference, we quantitatively explored the effects of ET, precipitation, and runoff on TWS changes in the Fenhe River Basin using partial correlations. The results showed that the increasing ET ($r = -0.79$, $p < 0.01$) and runoff ($r = -0.56$, $p < 0.01$) were significantly and negatively correlated with TWS decline (Fig. 6). In addition, partial correlations indicated that the relationship between ET and TWS remained significant after controlling for the effects of precipitation and runoff (Fig. 6), which suggested that the loss of TWS in the basin was mainly induced by the rapid increase of ET rather than the changes of precipitation and runoff.

To further clarify the reason for ET increases, we investigated the interannual variations of irrigation water use in the basin and found that the average annual irrigation water use during ER was lower than that before ER (Fig. 5e), which suggested that the changes in irrigation water use were not the main contributor of ET increases during ER. The most rapid increases in temperature occurred in the provinces of Henan and Shandong, rather than the basin and Shanxi Province (Figure S7). The above analyses revealed that ER programs greatly contributed to the rapid increases in ET and caused the decline of TWS in the hotspot during 2002–2016, which agreed with the recently published studies that ER led to the loss of freshwater resources through the ET process in China's Loess Plateau (Feng et al., 2016) and Mu Us Sandyland (Zhao et al., 2021).

Similar to the ER regions, NDVI (−0.002/yr), LAI (−0.02 m^2/m^2/yr), and ET (−11.9 mm/yr) in the hotspot also decreased before 1999 and then continuously and significantly ($p < 0.01$) increased (NDVI: 0.011/yr; LAI: 0.05 m^2/m^2/yr; ET: 8.7 mm/yr) (Fig. 7a–c). Furthermore, we explored the contributions of the changes of the three components (vegetation transpiration, canopy interception loss, and soil evaporation) to the variations of ET in the hotspot. Vegetation transpiration (8.25 mm/yr) and canopy interception loss (0.77 mm/yr) showed significantly increasing trends, while soil evaporation (2.68 mm/yr)

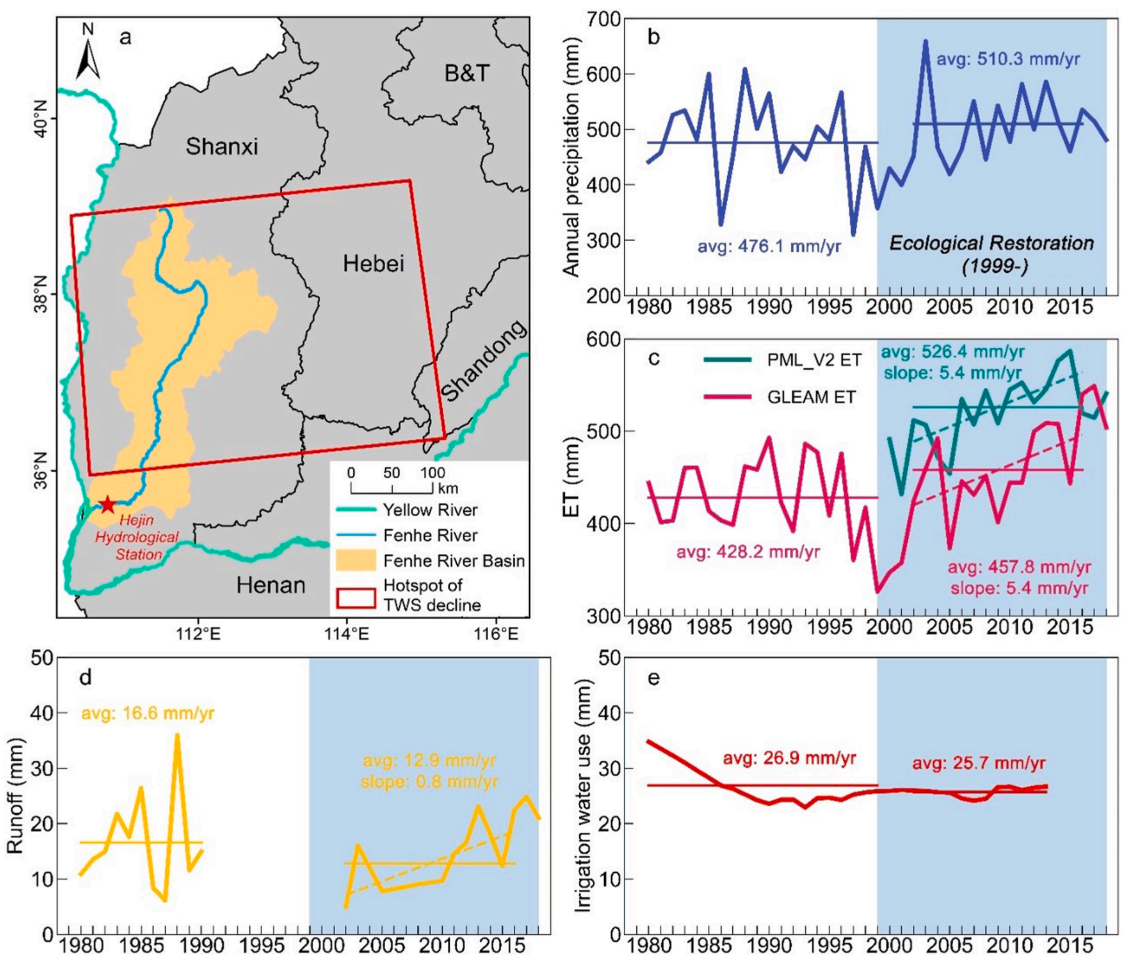

Fig. 5. Variations and trends of annual precipitation, ET, runoff, and irrigation water use in the Fenhe River Basin during 1980–2018. (a) The geographical location of the Fenhe River Basin, which is in the central part of the hotspot and involves the six prefectures of Xinzhou, Lvliang, Taiyuan, Jinzhong, Linfen, and Yuncheng in Shanxi Province; (b–e) Interannual variations of annual precipitation (CRU), ET (PML_V2 and GLEAM), runoff, and irrigation water use in the Fenhe River Basin during 1980–2018 and the linear trends of these factors during different periods.

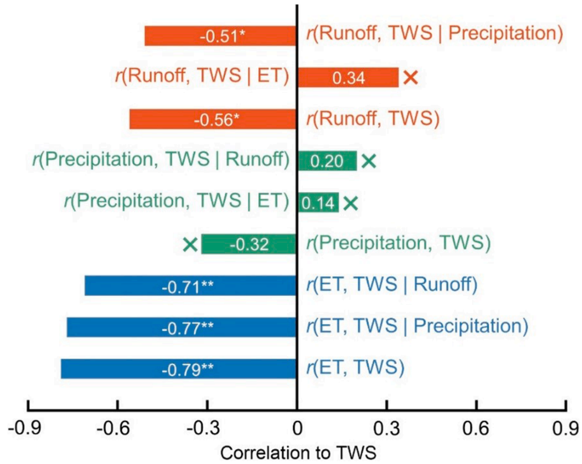

Fig. 6. Correlations and partial correlations between water balance components and TWS changes. Shown in blue, from bottom to top, is first the correlation between ET and TWS, followed by partial correlations *r* between ET and TWS after controlling for the effect of precipitation and runoff. Shown in green, from bottom to top, is first the correlation between precipitation and TWS, followed by partial correlations *r* between precipitation and TWS after controlling for the effect of ET and runoff. Shown in orange, from bottom to top, is first the correlation between runoff and TWS, followed by partial correlations *r* between runoff and TWS after controlling for the effect of ET and precipitation. Each cross symbol indicates that the trend was not statistically significant ($p \geq 0.05$). The symbols "*" and "**" represent the statistically significant correlations with $p < 0.05$ and $p < 0.01$, respectively.

showed decreasing trend (Fig. 7d–F). In addition, vegetation transpiration had the most rapid increase in the hotspot (Fig. 7g). By investigating the annual variations of vegetation canopy, soil evaporation, and interception loss in the ecological restoration region from 2000 to 2018 using different data layers in PML-V2 datasets (Fig. S8a), we found that the proportion of vegetation transpiration to ET continuously and significantly increased (1.02%/yr, $p < 0.01$) with an average value of 49.0% (Fig. S8b), suggesting that the increases in ET in the region were also mainly caused by the continuous increases in vegetation transpiration.

4. Discussion

4.1. ER exacerbates the agriculture-induced water crisis

As a typical grain bowl and highly populated and urbanized region in China, the NCR has been suffering from extreme water shortage due to intensive agricultural irrigation(Guo and Shen 2015; Qin et al., 2013; Zhou et al., 2022). Agriculture was the largest water use sector, much higher than residential and industrial water use. Despite increasing residential water use, the decreasing water consumption from agriculture alleviated the water crisis in the past decades (Fig. 3). Previous studies have demonstrated that the ER-induced greening was at the expense of water resources due to rapid ET increases and caused severe water depletion in the Loess Plateau (Feng et al., 2016; Shao et al., 2019) and Mu Us Sandyland (Zhao et al., 2021) of China. In this study, we also found that afforestation has significantly caused the increases in vegetation growth and subsequently ET in the western NCR that experienced large-scale implementation of ER programs (i.e., Grain to Green Program and Natural Forest Conservation Program). The accelerated ecological water consumption has caused the rapid loss of TWS in the region, especially in the hotspot. While the considerable impacts of long-term agricultural irrigation on water storage in the NCR have been well documented in previous studies (Aeschbach-Hertig and Gleeson 2012; Feng et al., 2013; Huang et al., 2015; Qin et al., 2013), this study proved that ER programs were posing a new threat to water security and exacerbating the water shortage originally caused by agriculture in the NCR. In the regions experiencing ER programs and TWS depletion, reevaluating the hydrologic impacts of afforestation will be important to relieve water pressure.

4.2. Potential effects of future climate on TWS

Whether the decline of TWS in the ER regions will continue depends on the interactions between afforestation intensity and local meteorological conditions (Zhao et al., 2021). Future climate projection showed that precipitation in the NCR was likely to increase (0.52–1.19 mm/yr, $p < 0.01$) during 2020–2099 (Fig. 8a-b), which was consistent with findings from previous studies (Feng et al., 2016; Long et al., 2020). Projected precipitation increases suggested a higher possibility of TWS recovery in the future. Therefore, water consumption as afforestation would be alleviated to some degree with the increasing precipitation, and TWS depletion would remain stable or reversed. If afforestation intensifies, water consumption would surpass the recharge from precipitation, and TWS decline would be accelerated. The CMIP5 projected data revealed that the annual mean temperature would significantly increase (0.02–0.06 °C/yr) in the future (Fig. 8c-d). Future wetting and warming are expected to promote both TWS replenishment and plant growth, which will probably provide more room for ER to function under a low level of ER efforts and fovour a strategy with reduced human revegetation but more nature regeneration (Zhao et al., 2021). In addition, it should be noted that plant water-use efficiency could increase under rising greenhouse gas concentrations (Donohue et al., 2013; Wullschleger et al., 2002). Feng et al. (2016) projected an average increase of water-use efficiency of 10% by 2050 using multiple CMIP5 land surface models (Feng et al., 2016), which might partly ameliorate the negative effects of increasing temperature on plant transpiration. In general, climate conditions in the coming decades favor TWS recovery if the afforestation intensity is no longer enhanced. Future studies should focus on more comprehensive and quantitative analyses of future trends of TWS by fully considering ER strategies, local hydrometeorological conditions, plant water use, etc.

4.3. Potential measures to promote sustainable development in the NCR

The decline of water storage has brought significant threats to food, water, and ecological securities in the NCR, which are closely related to Target 2 (Zero Hunger), 6 (Clean Water and Sanitation), and 15 (Life on Land) of the sustainable development goals (SDGs), respectively. The synergetic development of the three closely related SDG indicators is critical for NCR's sustainable development. The interactions between water-food-ecology are complex (Filoso et al., 2017; Karabulut et al., 2016). In the permanent agricultural areas widely distributed in the central and eastern parts of the NCR, excessive groundwater pumping for irrigation in the past decades caused severe TWS depletion, which has been reported in previous studies (Feng et al., 2013; Huang et al., 2015; Pan et al., 2017; Qin et al., 2013). While the large-scale implementation of ER programs since 1999 enhanced vegetation growth and improved ecological security in the western NCR, it brought considerable threats to water security and exacerbated the water crisis originally induced by agricultural irrigation in the NCR. The conflicts in water consumption between agriculture and ecological service maintenance tend to be aggravated. Therefore, more comprehensive strategies considering water, food, and ecological securities are urgently needed to instruct the balance of different SDGs to promote sustainable development in the NCR (Aeschbach-Hertig and Gleeson 2012).

More scientific and effective measures need to be considered to reverse the TWS depletion trend in the NCR. In addition to improving the efficiency of agricultural water use to release water shortage in the major agricultural production areas (Blanke et al., 2007), more adaptive approaches to reduce ecological water consumption in the ER regions are urgently needed to achieve regional sustainable development.

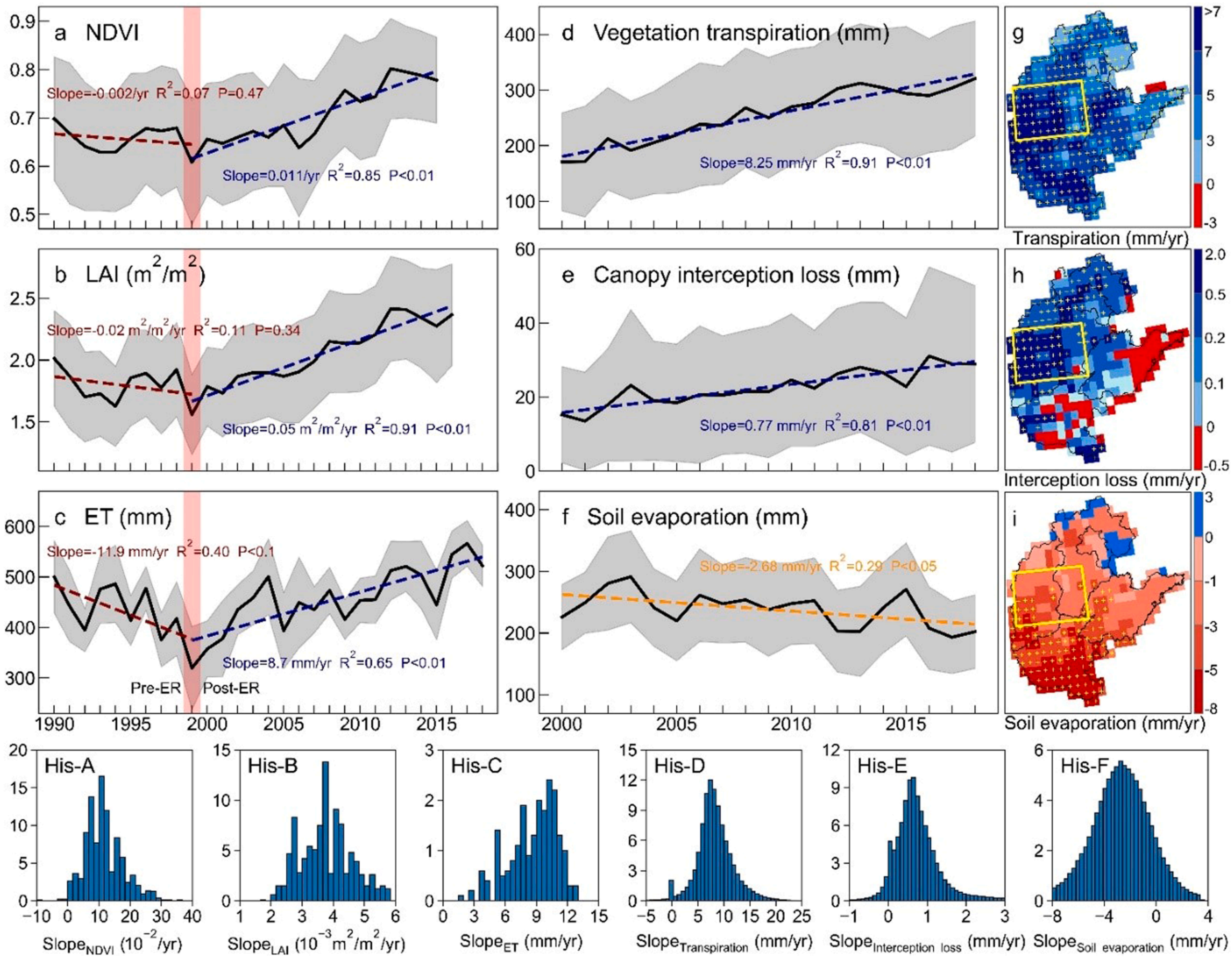

Fig. 7. Variations and trends of NDVI, LAI, and ET in the hotspot. (a–c) Interannual variations and trends of NDVI (GIMMS-3 g), LAI (mean of GLASS, GLOBMAP, and LAI3g), and ET (GLEAM) in the hotspot during 1990–2018; (d–f) Interannual variations and trends of vegetation transpiration, canopy interception loss, and soil evaporation derived from PML-V2 datasets in the hotspot during 2000–2018; (g–i) Spatial patterns of linear trends of vegetation transpiration, canopy interception loss, and soil evaporation in the hotspot during 2000–2018. The symbol "+" in each grid cell indicates a statistically significant trend with a p-value < 0.05. The below shows the histograms (a–f) of the slopes in the linear trends of these indicators (a–c: 1999–2018; d–f: 2000–2018).

Reducing ER efforts and regulating plant water uptake by thinning densely vegetated regions is the key to relieving the loss of water storage. Both ecosystems and human activities consume the same source of freshwater (Feng et al., 2016). Though afforestation significantly improves the ecological environment in the ER regions, ecological water use should be maintained lower than the allowable threshold to realize the balance of water consumption between ecological protection and socioeconomic development (Feng et al., 2016). Replacing the current tree species with those with less ET is a good choice for promoting the synergetic development between freshwater resources protection and ecological security in the ER regions. The current vegetation species in the hotspot are dominated by shrubs (e.g., *Pinus tabuliformis Carr.* and *Robinia pseudoacacia*) and trees (e.g., *Periploca sepium Bunge and Rosa xanthine Lindl.*) (Feng et al., 2016; Han et al., 2021; Jia et al., 2017; McVicar et al., 2010). However, compared with shrubs, *Robinia pseudoacacia* has higher transpiration because it consumes large amounts of water from deep soil layers (Jia et al., 2017; McVicar et al., 2010; Sankaran et al., 2005; Wang et al., 2008). Therefore, it could be a potential measure to replace *Robinia pseudoacacia* with shrubs, which have a lower water requirement for survival (McVicar et al., 2010). In addition, using water from outside river basins by water diversion projects other than local freshwater resources is another effective solution for protecting groundwater. For example, since the operation of the middle route of the South-to-North Water Diversion project in 2014, 9.5 km^3 of water from the Yangtze River has been annually transported to the NCR, which has reduced cumulative groundwater depletion by ~3.6 km^3 in Beijing and has greatly relieved water shortage there (Long et al., 2020; Qin et al., 2012; Yang et al., 2022; Zhang et al., 2020).

4.4. Uncertainty analyses and effects of coal mining on GRACE TWS

Although the current research, together with previous studies (Bai et al., 2020; Feng et al., 2016; Zhao et al., 2021), have contributed to the knowledge of the significant effects of ER programs on regional water resources, we have to recognize that there are still uncertainties remained in the analytical methods and remote sensing data used. Firstly, there will inevitably be deviations between remote sensing observations and field surveys regarding the ecological indicators (van Leeuwen et al. 2006). Zhang et al. (2013) demonstrated that the integration of different kinds of NDVI data sets (e.g., MODIS and GIMMS-3 g) would better address issues of uncertainty related to remote sensing applications in vegetation change studies, here we also applied various data to examine the trends of ecological indicators (i.e., NDVI, LAI, and ET) and climate factors (i.e., temperature and precipitation) to reduce the uncertainties. Secondly, we aggregated the data of ecological indicators into 0.5° raster data by using an arithmetic mean method to

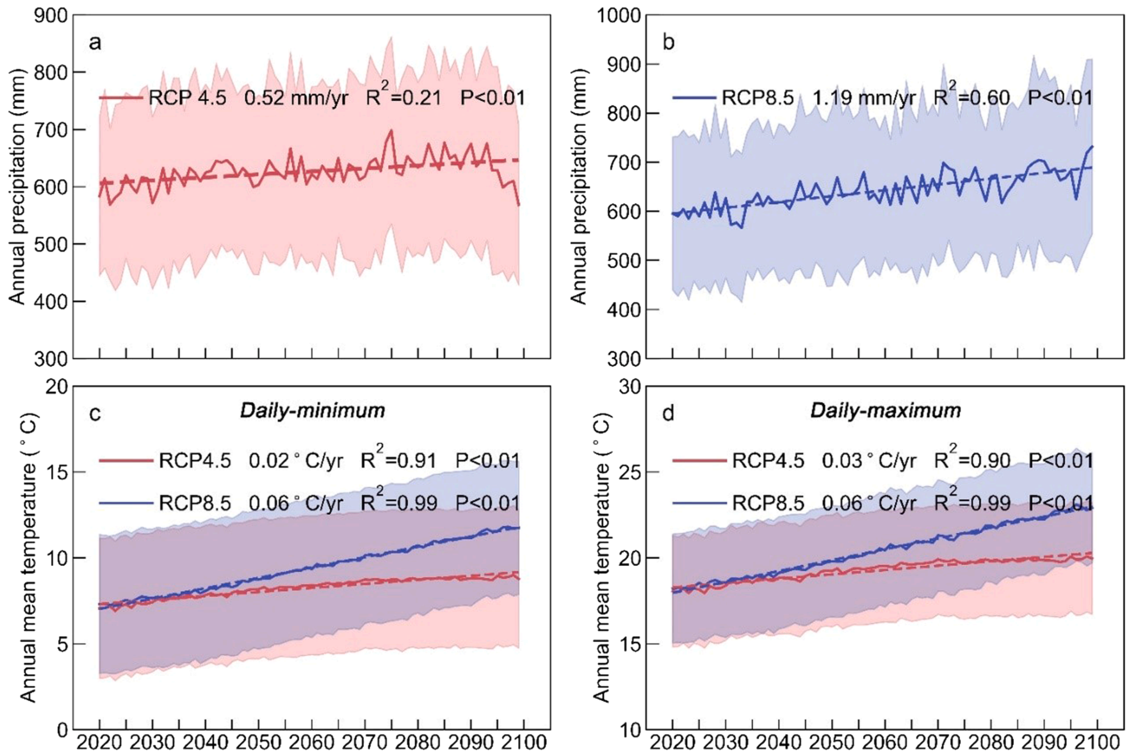

Fig. 8. Future climate projection in the NCR from 2020 to 2099. Variations and trends of annual precipitation based on the CMIP5 projected data under both scenarios of RCP 4.5 (a) and RCP 8.5 (b); Variations and trends of the annual mean temperature of daily-minimum (c) and daily-maximum (d) under both scenarios of RCP 4.5 and RCP 8.5.

investigate the spatial patterns of linear trends of these indicators. However, previous studies (Chen 1999; Jiang et al., 2006) showed that such aggregation was likely to introduce uncertainties to the measurements of these indicators in heterogeneous surfaces because resampling could cause the attributes of pixels to change. Finally, annual 30-m yearlong water body maps used in this study, which were generated by Landsat data, could miss some water bodies with sizes smaller than 30 m × 30 m. However, our previous studies (Zhou et al., 2019; Zou et al., 2017) have revealed that the dynamics of areas of yearlong surface water were mainly caused by the changes in large water bodies (e.g., lakes and reservoirs), which could be accurately detected by Landsat.

GRACE detects combined mass changes that include signals from hydrology, solid earth, cryosphere, ocean, atmosphere, and tides (Jacob et al., 2012; Wang et al., 2013). Although the non-hydrologic signals are removed as far as possible in the GRACE TWS estimates (Landerer and Swenson 2012), the signals of anthropogenic mass flow (e.g., coal mining and transportation) are not considered during the data processing (Tang et al., 2013). Therefore, in the regions with intense mineral exploitation (e.g., Shanxi Province), TWS changes detected by the GRACE satellite could be affected by the dynamics of anthropogenic mass flow. Tang et al. (2013) showed that a huge amount of coal produced by Shanxi Province has been transported to coastal demand centers such as Shanghai and Hong Kong. The accumulated net coal exportation in the western NCR reached 6.6 billion tons from 2003 to 2011, equivalent to a loss of TWS of 28.5 mm (Tang et al., 2013). Similarly, we also revealed that coal mining and its cumulative equivalent water thickness (59.5 mm) were the highest in Shanxi (Fig. 9a–e) and accounted for 39.0% of the total mass losses, which were roughly equivalent to water storage of 24.2 km^3 in the province during 2003–2015 (Fig. 9f). Especially in the hotspot, the cumulative equivalent water thickness of coal mining during 2003–2015 reached 70.0 mm at an average rate of 5.4 mm/yr (Fig. 9g), accounting for 41.0% of the total mass losses in the region in the period (Fig. 9h). Therefore, the actual rate of TWS decline in the hotspot was about 7.3 mm/yr, which was close to the rate of ET increase (8.7 mm/yr) and could better support our conclusion that the increasing water consumption through ET was the major driver for TWS depletion.

5. Conclusion

The NCR is a typical grain base and highly populated and urbanized area in China. As a well-recognized global groundwater funnel, the region has been suffering from severe water shortage in the past decades. Using three kinds of GRACE satellite data sets and the GEE cloud computing platform, the current study investigated the interannual variations and trends of TWS from 2002 to 2016. The results showed that TWS showed continuously decreasing trends (−8.9 mm/yr) in the NCR during the period. The most rapid decline of TWS (−12.7±0.45 mm/yr) happened in the western part of NCR, which was the hotspot of depleted TWS identified in this study. At the provincial scale, Shanxi experienced the most rapid loss in TWS (−11.7 mm/yr), followed by Hebei (−10.2 mm/yr), B&T (−9.7 mm/yr), Shandong (−8.4 mm/yr), and Henan (−5.2 mm/yr). The rate of TWS decline (−11.7 mm/yr) in the NCR during 2004–2016 was higher than that during 2002–2016 as there was a sharp increase in TWS from 2002 to 2004 due to the highest recorded annual precipitation in 2003 and the implementation of water projects. We found that the western and northern parts of NCR experienced substantial reforestation as the result of the large-scale implementation of ER programs (i.e., Grain to Green Program and Natural Forest Conservation Program), and the interannual variations and spatial patterns of TWS depletion are consistent with those ER-induced greening. Attribution analyses of TWS depletion by fully considering precipitation, ET, and runoffs suggested that increasing ET was the major driver for TWS depletion in the ER regions. This study warned that ER programs were posing a new threat to water security and exacerbating the water crisis originally induced by agriculture in the NCR, and effective measures were urgently needed to achieve the synergy of food, water, and ecological securities and regional sustainable development.

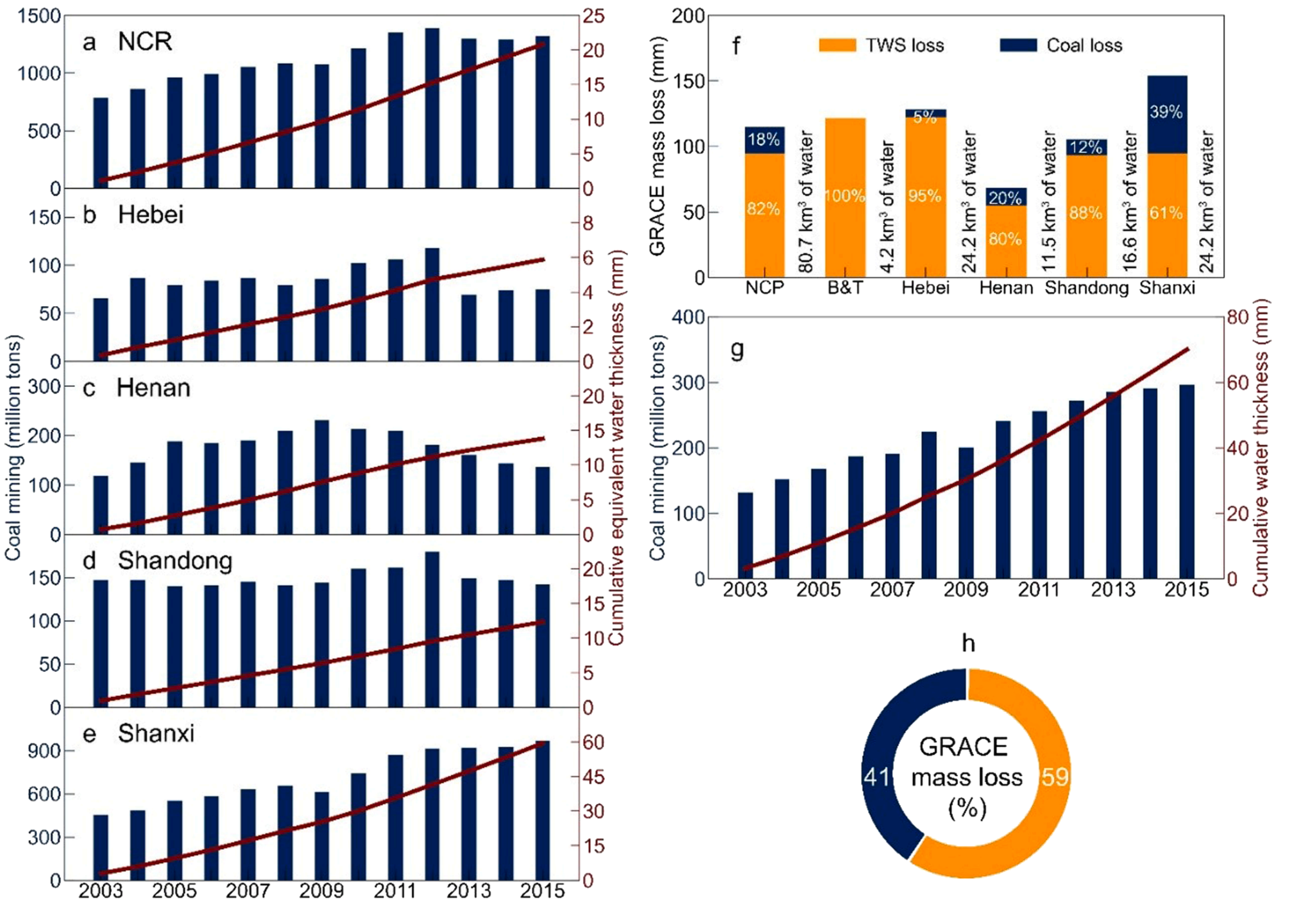

Fig. 9. Effects of coal mining on mass losses derived from GRACE. (a–e) Variations of coal mining and its cumulative equivalent water thickness in the entire NCR and each province during 2003–2015; (f) Percentages of mass losses from coal mining and TWS relative to the total mass losses derived from GRACE in the entire NCR and each province from 2003 to 2015; (g) Variations of coal mining and its cumulative equivalent water thickness in the overlapping region of the hotspot and Shanxi Province during 2003–2015; (h) Percentage of coal mining relative to the mass losses in the overlapping region from 2003 to 2015.

Declaration of Competing Interest

The authors declare that they have no known competing financial interests or personal relationships that could have appeared to influence the work reported in this paper.

Data availability

Data will be made available on request.

Acknowledgments

This research was funded by the National Natural Science Foundation of China (42271375 and 42071415), the Strategic Priority Research Program (XDA28060100) and the Youth Interdisciplinary Team Project (JCTD-2021-04) of the Chinese Academy of Sciences (CAS), and the Outstanding Youth Foundation of Henan Natural Science (202300410049).

Supplementary materials

Supplementary material associated with this article can be found, in the online version, at doi:10.1016/j.agrformet.2023.109341.

References

Aeschbach-Hertig, W., Gleeson, T., 2012. Regional strategies for the accelerating global problem of groundwater depletion. Nat. Geosci. 5 (12), 853–861.
Asoka, A., Gleeson, T., Wada, Y., Mishra, V., 2017. Relative contribution of monsoon precipitation and pumping to changes in groundwater storage in India. Nat. Geosci. 10 (2), 109–117.
Bai, P., Liu, X., Zhang, Y., Liu, C., 2020. Assessing the impacts of vegetation greenness change on evapotranspiration and water yield in China. Water Resour. Res. 56 (10) e2019WR027019.
Bennett, M.M., Smith, L.C., 2017. Advances in using multitemporal night-time lights satellite imagery to detect, estimate, and monitor socioeconomic dynamics. Remote Sens. Environ. 192, 176–197.
Blanke, A., Rozelle, S., Lohmar, B., Wang, J., Huang, J., 2007. Water saving technology and saving water in China. Agricul. Water Manag. 87 (2), 0–150.
Bryan, B.A., Gao, L., Ye, Y., Sun, X., Connor, J.D., Crossman, N.D., et al., 2018. China's response to a national land-system sustainability emergency. Nature 559 (7713), 193–204.
Chen, C., Park, T., Wang, X., Piao, S., Xu, B., Chaturvedi, R.K., et al., 2019a. China and India lead in greening of the world through land-use management. Nat. Sustainabil. 2 (2), 122–129.
Chen, J.M., 1999. Spatial scaling of a remotely sensed surface parameter by Contexture. Remote Sens. Environ. 69 (1), 30–42.
Chen, J.M., Ju, W.M., Ciais, P., Viovy, N., Liu, R.G., Liu, Y., et al., 2019b. Vegetation structural change since 1981 significantly enhanced the terrestrial carbon sink. Nat. Commun. 10.
Döll, P., Müller Schmied, H., Schuh, C., Portmann, F.T., Eicker, A., 2014. Global-scale assessment of groundwater depletion and related groundwater abstractions: combining hydrological modeling with information from well observations and GRACE satellites. Water Resour. Res. 50 (7), 5698–5720.
Dong, N., Wei, J., Yang, M., Yan, D., Yang, C., Gao, H., et al., 2022. Model estimates of china's terrestrial water storage variation due to reservoir operation. Water Resour. Res. 58 (6) e2021WR031787.
Donohue, R.J., Roderick, M.L., McVicar, T.R., Farquhar, G.D., 2013. Impact of CO2 fertilization on maximum foliage cover across the globe's warm, arid environments. Geophys. Res. Lett. 40 (12), 3031–3035.

Feng, W., Zhong, M., Lemoine, J.M., Biancale, R., Hsu, H.T., Xia, J., 2013. Evaluation of groundwater depletion in North China using the gravity recovery and climate experiment (GRACE) data and ground-based measurements. Water Resour. Res. 49 (4), 2110–2118.
Feng, X., Fu, B., Piao, S., Wang, S., Ciais, P., Zeng, Z., et al., 2016. Revegetation in China's Loess Plateau is approaching sustainable water resource limits. Nat. Clim. Chang. 6, 1019–1022.
Filoso, S., Bezerra, M.O., Weiss, K.C.B., Palmer, M.A., 2017. Impacts of forest restoration on water yield: a systematic review. PLoS One 12 (8).
Forkel, M., Migliavacca, M., Thonicke, K., Reichstein, M., Schaphoff, S., Weber, U., et al., 2015. Codominant water control on global interannual variability and trends in land surface phenology and greenness. Glob. Chang Biol. 21 (9), 3414–3435.
Gong, P., Li, X., Wang, J., Bai, Y., Chen, B., Hu, T., et al., 2020. Annual maps of global artificial impervious area (GAIA) between 1985 and 2018. Remote Sens. Environ. 236, 111510.
Greve, P., Kahil, T., Mochizuki, J., Schinko, T., Satoh, Y., Burek, P., et al., 2018. Global assessment of water challenges under uncertainty in water scarcity projections. Nat. Sustainab. 1 (9), 486–494.
Guo, Y., Shen, Y.J., 2015. Quantifying water and energy budgets and the impacts of climatic and human factors in the Haihe River Basin, China: 1. Model and validation. J. Hydrol. (Amst) 528, 206–216.
Han, L., Yang, F., Wu, Y., Niu, Y., Zeng, Y., Chen, L., 2021. Responses of short-term water use efficiency to environmental factors in typical trees and shrubs of the loess area in West Shanxi, China. Chinese J. Plant Ecol. 45 (12), 1350–1364.
Han, S.J., Tian, F.Q., Liu, Y., Duan, X.H., 2017. Socio-hydrological perspectives of the co-evolution of humans and groundwater in Cangzhou, North China Plain. Hydrol. Earth Syst. Sci. 21 (7), 3619–3633.
He, C., Liu, Z., Wu, J., Pan, X., Fang, Z., Li, J., et al., 2021a. Future global urban water scarcity and potential solutions. Nat. Commun. 12 (1), 4667.
He, X., Bryant, B.P., Moran, T., Mach, K.J., Wei, Z., Freyberg, D.L., 2021b. Climate-informed hydrologic modeling and policy typology to guide managed aquifer recharge. Sci. Adv. 7 (17), eabe6025.
Huang, H., 2003. Analysis of Ecological Urgent Water Replenishing From the Yangtze River to Nansihu Lake. South-to-North Water Transf. Water Sci. Technol. 1, 22–25.
Huang, Z.Y., Pan, Y., Gong, H.L., Yeh, P.J.F., Li, X.J., Zhou, D.M., et al., 2015. Subregional-scale groundwater depletion detected by GRACE for both shallow and deep aquifers in North China Plain. Geophys. Res. Lett. 42 (6), 1791–1799.
Jacob, T., Wahr, J., Pfeffer, W.T., Swenson, S., 2012. Recent contributions of glaciers and ice caps to sea level rise. Nature 482 (7386), 514–518.
Jia, X., Shao, M.a., Zhu, Y., Luo, Y., 2017. Soil moisture decline due to afforestation across the Loess Plateau, China. J. Hydrol. 546, 113–122.
Jia, Y., Li, C., Yang, H., Yang, W., Liu, Z., 2022. Assessments of three evapotranspiration products over China using extended triple collocation and water balance methods. J. Hydrol. (Amst) 614, 128594.
Jiang, Z., Huete, A.R., Chen, J., Chen, Y., Li, J., Yan, G., et al., 2006. Analysis of NDVI and scaled difference vegetation index retrievals of vegetation fraction. Remote Sens. Environ. 101 (3), 366–378.
Karabulut, A., Egoh, B.N., Lanzanova, D., Grizzetti, B., Bidoglio, G., Pagliero, L., et al., 2016. Mapping water provisioning services to support the ecosystem-water-food-energy nexus in the Danube river basin. Ecosyst. Services 17, 278–292.
Koch, J., Zhang, W., Martinsen, G., He, X., Stisen, S., 2020. Estimating net irrigation across the North China Plain through dual modeling of evapotranspiration. Water Resour. Res. 56 (12) e2020WR027413.
Landerer, F.W., Swenson, S.C., 2012. Accuracy of scaled GRACE terrestrial water storage estimates. Water Resour. Res. 48, W04531.
Li, C., Zhang, Y., Shen, Y., Kong, D., Zhou, X., 2020a. LUCC-Driven changes in gross primary production and actual evapotranspiration in Northern China. J. Geophys. Res.: Atmospheres 125 (6) e2019JD031705.
Li, X., Zhou, Y., Zhao, M., Zhao, X., 2020b. A harmonized global nighttime light dataset 1992–2018. Sci. Data 7 (1), 168.
Li, Y., Piao, S., Li, L.Z.X., Chen, A., Wang, X., Ciais, P., et al., 2018. Divergent hydrological response to large-scale afforestation and vegetation greening in China. Sci. Adv. 4 (5), eaar4182.
Liang, S.L., Zhao, X., Liu, S.H., Yuan, W.P., Cheng, X., Xiao, Z.Q., et al., 2013. A long-term global land surface satellite (GLASS) data-set for environmental studies. Int. J. Digital Earth 6, 5–33.
Liu, J., Kuang, W., Zhang, Z., Xu, X., Qin, Y., Ning, J., et al., 2014. Spatiotemporal characteristics, patterns, and causes of land-use changes in China since the late 1980s. J. Geograph. Sci. 24 (2), 195–210.
Liu, J., Li, S., Ouyang, Z., Tam, C., Chen, X., 2008. Ecological and socioeconomic effects of China's policies for ecosystem services. Proc. Natl. Acad. Sci. U.S.A. 105 (28), 9477–9482.
Liu, J., Liu, M., Zhuang, D., Zhang, Z., Deng, X., 2003. Study on spatial pattern of land-use change in China during 1995–2000. Earth Sci. 46 (4), 373–384.
Liu, J., Ning, J., Kuang, W., Xu, X., Zhang, S., Yan, C., et al., 2018. Spatio-temporal patterns and characteristics of land-use change in China during 2010-2015. Acta Geogr. Sin. 73 (5), 789–802.
Liu, J., & Yang, W. (2012). Water sustainability for china and beyond. Science.
Liu, J., Zhang, Z., Xu, X., Kuang, W., Zhou, W., Zhang, S., et al., 2010. Spatial patterns and driving forces of land use change in China during the early 21st century. J. Geograph. Sci. 20 (4), 483–494.
Liu, Y., Liu, R.G., Chen, J.M., 2012. Retrospective retrieval of long-term consistent global leaf area index (1981-2011) from combined AVHRR and MODIS data. J. Geophys. Res. Biogeosci. 117, G04003.
Long, D., Yang, W., Scanlon, B.R., Zhao, J., Liu, D., Burek, P., et al., 2020. South-to-North Water Diversion stabilizing Beijing's groundwater levels. Nat. Commun. 11, 3665.
Lu, F., Hu, H., Sun, W., Zhu, J., Liu, G., Zhou, W., et al., 2018. Effects of national ecological restoration projects on carbon sequestration in China from 2001 to 2010. Proc. Natl. Acad. Sci. U.S.A. 115 (16), 4039–4044.
Ma, T., Sun, S., Fu, G., Hall, J.W., Ni, Y., He, L., et al., 2020. Pollution exacerbates China's water scarcity and its regional inequality. Nat. Commun. 11 (1), 650.
Martens, B., Miralles, D.G., Lievens, H., van der Schalie, R., de Jeu, R.A.M., Fernandez-Prieto, D., et al., 2017. GLEAM v3: satellite-based land evaporation and root-zone soil moisture. Geoscient. Model Develop. 10 (5), 1903–1925.
McVicar, T.R., Van Niel, T.G., Li, L., Wen, Z., Yang, Q., Li, R., et al., 2010. Parsimoniously modelling perennial vegetation suitability and identifying priority areas to support China's re-vegetation program in the Loess Plateau: matching model complexity to data availability. For. Ecol. Manage. 259 (7), 1277–1290.
Meng, F., Su, F., Li, Y., Tong, K., 2019. Changes in terrestrial water storage during 2003–2014 and possible causes in Tibetan Plateau. J. Geophys. Res. 124 (6), 2909–2931.
Ouyang, Z., Zheng, H., Xiao, Y., Polasky, S., Liu, J., Xu, W., et al., 2016. Improvements in ecosystem services from investments in natural capital. Science 352 (6292), 1455–1459.
Pan, Y., Zhang, C., Gong, H.L., Yeh, P.J.F., Shen, Y.J., Guo, Y., et al., 2017. Detection of human-induced evapotranspiration using GRACE satellite observations in the Haihe River basin of China. Geophys. Res. Lett. 44 (1), 190–199.
Qin, H., Cao, G., Kristensen, M., Refsgaard, J.C., Rasmussen, M.O., He, X., et al., 2013. Integrated hydrological modeling of the North China Plain and implications for sustainable water management. Hydrol. Earth Syst. Sci. 17 (10), 3759–3778.
Qin, H., Sun, A., Liu, J., Zheng, C., 2012. Evaluation of Land Surface Models in Reproducing Satellite Derived Leaf Area Index over the High-Latitude Northern Hemisphere. Part II: Earth Syst. Models. Water Policy 14, 214–231.
Ramillien, G., Frappart, F., Guntner, A., Ngo-Duc, T., Cazenave, A., Laval, K., 2006. Time variations of the regional evapotranspiration rate from Gravity Recovery and Climate Experiment (GRACE) satellite gravimetry. Water Resour. Res. 42 (10), W10403.
Rodell, M., Famiglietti, J.S., Wiese, D.N., Reager, J.T., Beaudoing, H.K., Landerer, F.W., et al., 2018. Emerging trends in global freshwater availability. Nature 557 (7707), 651–659.
Rodell, M., Velicogna, I., Famiglietti, J.S., 2009. Satellite-based estimates of groundwater depletion in India. Nature 460 (7258), 999–1002.
Sakumura, C., Bettadpur, S., Bruinsma, S., 2014. Ensemble prediction and intercomparison analysis of GRACE time-variable gravity field models. Geophys. Res. Lett. 41 (5), 1389–1397.
Sankaran, M., Hanan, N.P., Scholes, R.J., Ratnam, J., Augustine, D.J., Cade, B.S., et al., 2005. Determinants of woody cover in African savannas. Nature 438 (7069), 846–849.
Shao, R., Zhang, B., Su, T., Long, B., Cheng, L., Xue, Y., et al., 2019. Estimating the Increase in Regional Evaporative Water Consumption as a Result of Vegetation Restoration Over the Loess Plateau, China. J. Geophys. Res. 124 (22), 11783–11802.
Shen, Z., Zhang, Q., Singh, V.P., Pokhrel, Y., Li, J., Xu, C.Y., et al., 2022. Drying in the low-latitude Atlantic Ocean contributed to terrestrial water storage depletion across Eurasia. Nat. Commun. 13 (1), 1849.
Tang, Q.H., Zhang, X.J., Tang, Y., 2013. Anthropogenic impacts on mass change in North China. Geophys. Res. Lett. 40 (15), 3924–3928.
Tao, S., Fang, J., Ma, S., Cai, Q., Xiong, X., Tian, D., et al., 2019. Changes in China's lakes: climate and human impacts. Natl. Sci. Rev. 7 (1), 132–140.
Tucker, C.J., Pinzon, J.E., Brown, M.E., Slayback, D.A., Pak, E.W., Mahoney, R., et al., 2005. An extended AVHRR 8-km NDVI dataset compatible with MODIS and SPOT vegetation NDVI data. Int. J. Remote Sens. 26 (20), 4485–4498.
van Leeuwen, W.J.D., Orr, B.J., Marsh, S.E., Herrmann, S.M., 2006. Multi-sensor NDVI data continuity: uncertainties and implications for vegetation monitoring applications. Remote Sens. Environ. 100 (1), 67–81.
Wang, H., Jia, L., Steffen, H., Wu, P., Jiang, L., Hsu, H., et al., 2013. Increased water storage in North America and Scandinavia from GRACE gravity data. Nat. Geosci. 6, 38–42.
Wang, L., Tian, F., Wang, Y., Wu, Z., Schurgers, G., Fensholt, R., 2018. Acceleration of global vegetation greenup from combined effects of climate change and human land management. Glob. Chang. Biol. 24 (11), 5484–5499.
Wang, L., Wang, Q., Wei, S., Shao, M.a., Li, Y., 2008. Soil desiccation for Loess soils on natural and regrown areas. For. Ecol. Manage. 255 (7), 2467–2477.
Wang, X., Xiao, X., Zou, Z., Dong, J., Li, B., 2020. Gainers and losers of surface and terrestrial water resources in China during 1989–2016. Nat. Commun. 11 (1), 3471.
Wei, X., Ye, Y., Zhang, Q., Li, B., Wei, Z., 2019. Reconstruction of cropland change in North China Plain Area over the past 300 years. Glob Planet Change 176, 60–70.
Wullschleger, S.D., Tschaplinski, T.J., Norby, R.J., 2002. Plant water relations at elevated CO2– implications for water-limited environments. Plant Cell Environ. 25 (2), 319–331.
Xu, L., Chen, N.C., Zhang, X., Chen, Z.Q., 2019. Spatiotemporal changes in China's terrestrial water storage from GRACE satellites and its possible drivers. J. Geophys. Res. Atmospheres 124 (22), 11976–11993.
Yang, J., Dong, J., Xiao, X., Dai, J., Wu, C., Xia, J., et al., 2019. Divergent shifts in peak photosynthesis timing of temperate and alpine grasslands in China. Remote Sens. Environ. 233, 111395.
Yang, W., Long, D., Scanlon, B.R., Burek, P., Zhang, C., Han, Z., et al., 2022. Human intervention will stabilize groundwater storage across the North China Plain. Water Resour. Res. 58 (2) e2021WR030884.
Zhang, C., Duan, Q., Yeh, P.J.F., Pan, Y., Gong, H., Gong, W., et al., 2020. The effectiveness of the south-to-north water diversion middle route project on water delivery and groundwater recovery in North China Plain. Water Resour. Res. 56 (10) e2019WR026759.

Zhang, G., Zhang, Y., Dong, J., Xiao, X., 2013. Green-up dates in the Tibetan Plateau have continuously advanced from 1982 to 2011. Proceedings of the National Academy Sci. 110 (11), 4309–4314.
Zhang, Y., Kong, D., Gan, R., Chiew, F.H.S., McVicar, T.R., Zhang, Q., et al., 2019. Coupled estimation of 500 m and 8-day resolution global evapotranspiration and gross primary production in 2002-2017. Remote Sens. Environ. 222, 165–182.
Zhao, M., Aa, G., Zhang, J., Velicogna, I., Li, Z., 2021. Ecological restoration impact on total terrestrial water storage. Nat. Sustainabil. 4, 56–62.
Zhao, M., Zhou, Y., Li, X., Cheng, W., Zhou, C., Ma, T., et al., 2020. Mapping urban dynamics (1992–2018) in Southeast Asia using consistent nighttime light data from DMSP and VIIRS. Remote Sens. Environ. 248, 111980.
Zhou, F., Bo, Y., Ciais, P., Dumas, P., Tang, Q., Wang, X., et al., 2020. Deceleration of China's human water use and its key drivers. In: Proc. Natl. Acad. Sci. U.S.A., 117, pp. 7702–7711.
Zhou, Y., Dong, J., Cui, Y., Zhou, S., Li, Z., Wang, X., et al., 2022. Rapid surface water expansion due to increasing artificial reservoirs and aquaculture ponds in North China Plain. J. Hydrol. (Amst) 608, 127637.
Zhou, Y., Dong, J., Xiao, X., Liu, R., Zou, Z., Zhao, G., et al., 2019. Continuous monitoring of lake dynamics on the Mongolian Plateau using all available Landsat imagery and Google Earth Engine. Sci. Total Environ. 689, 366–380.
Zhou, Y., Li, X., Asrar, G.R., Smith, S.J., Imhoff, M., 2018. A global record of annual urban dynamics (1992–2013) from nighttime lights. Remote Sens. Environ. 219, 206–220.
Zhu, Z., Piao, S., Myneni, R.B., Huang, M., Zeng, Z., Canadell, J.G., et al., 2016. Greening of the earth and its drivers. Nat. Clim. Chang 6 (8), 791–795.
Zhu, Z.C., Bi, J., Pan, Y.Z., Ganguly, S., Anav, A., Xu, L., et al., 2013. Global data sets of vegetation leaf area index (LAI)3 g and fraction of photosynthetically active radiation (FPAR)3 g derived from global inventory modeling and mapping studies (GIMMS) normalized difference vegetation index (NDVI3g) for the period 1981 to 2011. Remote Sens (Basel) 5 (2), 927–948.
Zou, Z., Dong, J., Menarguez, M.A., Xiao, X., Qin, Y., Doughty, R.B., et al., 2017. Continued decrease of open surface water body area in Oklahoma during 1984–2015. Sci. Total Environ. 595, 451–460.
Zuo, L., Zhang, Z., Carlson, K.M., MacDonald, G.K., Brauman, K.A., Liu, Y., et al., 2018. Progress towards sustainable intensification in China challenged by land-use change. Nat. Sustainab. 1 (6), 304–313.